IOPscience iopscience.iop.org

Home Search Collections Journals About Contact us My IOPscience

Effect of hydrogen addition on the deposition of titanium nitride thin films in nitrogen added argon magnetron plasma

This content has been downloaded from IOPscience. Please scroll down to see the full text.

2016 J. Phys. D: Appl. Phys. 49 225203

(http://iopscience.iop.org/0022-3727/49/22/225203)

View the table of contents for this issue, or go to the journal homepage for more

Download details:

IP Address: 200.89.68.74

This content was downloaded on 12/08/2016 at 17:53

Please note that terms and conditions apply.

IOP Publishing Journal of Physics D: Applied Physics
J. Phys. D: Appl. Phys. **49** (2016) 225203 (10pp) doi:10.1088/0022-3727/49/22/225203

Effect of hydrogen addition on the deposition of titanium nitride thin films in nitrogen added argon magnetron plasma

P Saikia[1,2], H Bhuyan[2], D E Diaz-Droguett[2], F Guzman[3], S Mändl[4], B K Saikia[1], M Favre[2], J R Maze[2] and E Wyndham[2]

[1] Centre of Plasma Physics, Institute for Plasma Research, Nazirakhat, Sonapur, Kamrup, Assam 782402, India
[2] Instituto de Física, Pontificia Universidad Católica de Chile, Av. Vicuña Mackenna, 4860 Santiago, Chile
[3] Departamento de Física, Facultad de Ciencias Físicas y Matemáticas, Universidad de Chile, Av. Blanco Encalada, 2008 Santiago, Chile
[4] Leibniz Institut für Oberflächenmodifizierung, Permoserstr. 15, D-04318, Leipzig, Germany

E-mail: hbhuyan@fis.puc.cl

Received 4 November 2015, revised 23 March 2016
Accepted for publication 6 April 2016
Published 4 May 2016

Abstract
The properties and performance of thin films deposited by plasma assisted processes are closely related to their manufacturing techniques and processes. The objective of the current study is to investigate the modification of plasma parameters occurring during hydrogen addition in N_2 + Ar magnetron plasma used for titanium nitride thin film deposition, and to correlate the measured properties of the deposited thin film with the bulk plasma parameters of the magnetron discharge. From the Langmuir probe measurements, it was observed that the addition of hydrogen led to a decrease of electron density from 8.6 to 6.2 $\times$ (10^{14} m^{-3}) and a corresponding increase of electron temperature from 6.30 to 6.74 eV. The optical emission spectroscopy study reveals that with addition of hydrogen, the density of argon ions decreases. The various positive ion species involving hydrogen are found to increase with increase of hydrogen partial pressure in the chamber. The thin films deposited were characterized using standard surface diagnostic tools such as x-ray photoelectron spectroscopy (XPS), secondary ion mass spectrometry (SIMS), x-ray diffraction (XRD), Raman spectroscopy (RS), scanning electron microscopy (SEM) and energy dispersive x-ray spectroscopy (EDS). Although it was possible to deposit thin films of titanium nitride with hydrogen addition in nitrogen added argon magnetron plasma, the quality of the thin films deteriorates with higher hydrogen partial pressures.

Keywords: magnetron plasma, plasma parameters, titanium nitride thin film

(Some figures may appear in colour only in the online journal)

1. Introduction

Titanium nitride (TiN) has found a wide variety of applications in modern technology due to its distinctive physical, chemical and mechanical characteristics such as high hardness and elastic modulus, good wear and corrosion resistance and biocompatibility [1–8]. Because of their excellent bio-compatibility and corrosion resistant properties, TiN coated materials are often used for medical implants such as cement less total hip prosthesis [5–8]. The perspective of use of TiN coatings/films for different technological applications however is strongly related to their qualities and performances. Although, there exist various film deposition techniques, plasma deposition is often preferred for its productivity and

 © 2016 IOP Publishing Ltd Printed in the UK

simplicity. Over the last few years there has been a growing interest in the use of admixture gases like argon–hydrogen (Ar/H_2) in plasma deposition techniques. They have been used widely in cleaning and etching processes as the combination of chemical and physical etching process can lead to much higher rates than the single processes [9]. Recently, argon–hydrogen plasma is being considered in thin film deposition processes [10–18]. During the magnetron sputtering deposition of Al [10], gold [11] and carbon [12–14], argon–hydrogen plasma is used to avoid oxidation of the growing metal films. Furthermore, the use of hydrogen radicals as reducing agents to improve the density and crystallinity of transition metal nitrides thin films is reported in literature [15]. In contrast, H co-doping in magnetron sputter deposition of TiO_2 thin film permanently modifies its band structure by introducing Ti^{3+} impurity states while suppressing the formation of intrinsic deep defect states with consequences for the photocatalytic activity [16].

To study the plasma parameters of magnetron discharges, conventional techniques including Langmuir probes and optical emission spectroscopy (OES) are widely used [19–21]. The electron temperature (T_e), electron density (n_e) and ion density (n_i) can be measured using a Langmuir probe. By a suitable choice of different spectral lines of OES, it is possible to characterize different ionization and dissociation processes in the plasma. Recent findings speculate that the change of plasma parameters due to hydrogen addition in magnetron discharge will influence the properties of the deposited films, similar to other energetic PVD processes [22]. Therefore the diagnostics of the magnetron sputtering discharge deserves special attention and it is one of the prime aspects of this investigation. Keeping this fact in mind, the aim of the present investigation is to probe the modification of plasma parameters occurring during hydrogen addition in $N_2 + Ar$ magnetron plasma used for TiN thin film deposition and to correlate the properties of the deposited thin film with the bulk plasma parameters of the magnetron discharge. The nitrogen and argon gas partial pressure was kept fixed during the investigation, while hydrogen is added in a controlled manner. By keeping the nitrogen and the argon partial pressure constant, we eliminate the influence of the so called 'target poisoning effect' on the plasma parameters evaluation.

2. Experimental set-up

The experimental system used in this investigation is a 'Type 2 unbalanced magnetron'. An unbalanced magnetron is intentionally configured with magnetic pieces or coils that surround the central pole piece magnet. The central pole piece has been made much stronger than the perimeter pole piece, resulting in an additional axial magnetic field. In this case, some of the field lines are directed towards the substrate. Consequently, the plasma is no longer strongly confined to the target region but is allowed to flow out towards the substrate. Figure 1 shows a schematic diagram of the experimental arrangements for the deposition of TiN films and to investigate the plasma parameters as well as plasma species during deposition. A cylindrical vacuum chamber made of stainless steel

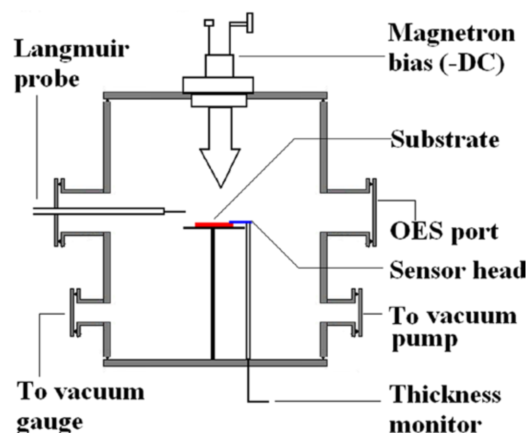

Figure 1. Schematic diagram of the experimental set-up.

304 mounted with a planar magnetron was used as the deposition setup. The chamber act as an anode in the steady state and its diameter and length are 350 mm and 400 mm, respectively. A water-cooled Ti target of diameter 70 mm was used as the cathode of the planar magnetron sputtering system.

The chamber is evacuated with a combination of diffusion pump (ULK-06 1000 lps) backed by a rotary pump (ULK-06 585 l min^{-1}) up to a base pressure of 6.5×10^{-6} mbar. A Baffle valve is provided to hinder the entry of oil vapors from the diffusion pump to the chamber during its operation. The Ti target was pre-sputtered in pure argon plasma before the deposition process, in order to remove the oxide layer on the target. A fall of magnetron bias voltage in the pre-sputtering period signifies the removal of oxide layer from the magnetron target. It is due to the fact that the magnetron target containing the oxide layer has lower value of ion induced secondary electron emission coefficient than the pure metallic target. Hence, a higher value of discharge current is expected upon the removal of oxide layer at the same discharge condition. Therefore to maintain the input power constant, there is a decrease of magnetron bias voltage. This fall of magnetron bias voltage is also associated with the change of discharge color. In our existing experimental set-up it takes around 10–15 min of pre-sputtering in pure argon plasma for the above mentioned changes. Although, it is not possible to figure out the exact amount of oxygen present in the form of oxide layer on the target, we believe that it was removed from the target surface during the pre-sputtering treatment. Commercially available one-sided mirror-like polished Si (1 0 0) substrates were mounted axially at a distance of 10 cm from the magnetron target. To avoid the exposure of the substrate to the plasma during the pre-sputtering period, a stainless steel shutter was placed in between the substrate and the target. The shutter was removed after the pre-sputtering period for the subsequent deposition, without disturbing the in vacuum conditions. For the deposition of TiN thin films on Si (1 0 0) substrate, argon (Ar), nitrogen (N_2) and hydrogen (H_2) were fed into the deposition chamber regulated by digital mass flow controllers (DFC 26, AALBORG USA). Here, nitrogen plays the role of reactive gas and small amounts of hydrogen is added to investigate its effect on the growth of TiN thin film as mentioned in the introduction section. A fixed argon and nitrogen partial pressure of 0.315 Pa and 0.035 Pa

(with a ratio 9:1) was maintained in all the deposition conditions. Hydrogen is then added gradually due to which the working pressure increases from 0.35 Pa (without hydrogen) up to 0.5 Pa (i.e. with 0.15 Pa H_2). The plasma parameters like electron temperature (T_e in eV), electron density (n_e) and ion density (n_i) were measured by a cylindrical Langmuir probe of length 3 mm and diameter 1 mm. The probe was placed in a region that was practically free of any magnetic field ($|B| \cong 0$) and is at a distance 10 mm above the substrate. The substrate holder has a diameter of 3 cm and thickness of 0.2 cm. To estimate the relative contribution of different ions in the plasma due to the mixing of different percentage of hydrogen gas in the nitrogen added argon plasma by measuring the intensity level of specific emission, a 1/2 m digikrom spectrometer (CVI Laser Corp, USA. Digikrom Model DK 480) is used. The system consists of a photo multiplier tube (PMT: Model AD110, wavelength range: 185–930 nm) and a grating with 1200 grooves mm^{-1} for detection in the region $\lambda = (400–850)$ nm. The entrance and exit slit of the monochromator were adjusted at 20 Å to obtain an acceptable spectral resolution sufficient to detect the emission lines. The emissions were collected by a light collecting system (LCS) through optical fiber (F) that was put on the glass window approximately at a vertical distance of 8 cm from the target in the downward region and kept in a manner to avoid background radiation as well as to detect maximum emission. The LCSF comprised of a plano-convex lens (diameter 2 mm, focal length 3 cm) and a silica fiber of 1.0 mm core (numerical aperture: 0.22). The view subtended by this LCS was parallel to the discharge column grazing the vicinity of the substrate and always collected radiations from the fixed location.

We took both the OES and Langmuir probe measurements near the substrate while keeping in mind that the electron and ion density in the vicinity of the substrate can significantly affect the physical properties of the deposited film [23]. A Crystal Thickness Monitor (DTM-101) manufactured by HIND-HIVAC, monitored the deposition rate at the discharge conditions. The monitor head was placed at the same horizontal plane as the substrate holder. Addition of hydrogen to Ar/N_2 magnetron discharge decreases the sputtering rate from 2.6 Å s^{-1} to 2.1 Å s^{-1} and results in TiN thin films of 470–380 nm thickness for 30 min of deposition.

The substrates were subsequently investigated under x-ray photoelectron spectroscopy (XPS), secondary ion mass spectrometry (SIMS), x-ray diffraction (XRD), Raman spectroscopy (RS), scanning electron microscopy (SEM), and energy dispersive x-ray spectroscopy (EDS). The surface chemistry of the TiN coated substrates was obtained by XPS (Physical Electronics systems model 1257) using Al $K\alpha$ emission. Binding energies and oxidation states were obtained from high resolution scans. The binding energy scale was calibrated according to the C 1*s* peak (284.8 eV) of adventitious carbon. The time-of-flight SIMS measurements were used to obtain the elemental depth profiles using 15 keV $^{69}Ga^+$ ions for the analysis and 2 keV cesium ions for sputter profiling. The respective scan areas were 100×100 and 300×300 μm^2 to avoid crater edge effects. The analysis current was about 2 pA with the sputter current around 100 nA, resulting in a surface removal rate of about 0.5 nm s^{-1} for the selected scan size. By measuring the crater depth, the thickness of the coated layers was determined by assuming a linear sputter rate with no degradation of the profile edges due to sputter roughening within the crater. The phase composition of the treated samples were studied by using a XRD3000PTS diffractometer with the Cu–$K\alpha$ radiation ($\lambda = 1.5406$ Å) in the Bragg–Brentano configuration operated at 40 keV and 50 mA. Unpolarized visible RS were obtained with a LabRam 010 instrument from ISA using a He–Ne laser (632.8 nm). The SEM studies were performed on a LEO 1420-VP Electron Microscopy operated at 20 kV and the EDS analysis were performed on an Oxford Instruments INCA X-Sight 7424 attached to the SEM.

Table 1. Current and voltage values in the discharge at various discharge conditions.

Working pressure (Pa)	Hydrogen partial pressure (Pa)	Voltage (V)	Current (mA)
3.5×10^{-1}	0	580	520
4×10^{-1}	0.5×10^{-1}	592	503
4.5×10^{-1}	1.0×10^{-1}	601	496
5×10^{-1}	1.5×10^{-1}	610	461

3. Results and discussions

3.1. Plasma characterization

With the addition of hydrogen to the nitrogen added argon plasma, a decrease of discharge current from 520 mA to 461 mA was observed. Consequently, an increase of discharge voltage for fixed input power of 300 W was noticed. For processes operated at a constant power, the observation of an increase in target voltage must be accompanied by a corresponding decrease in the ion current or in the secondary electron coefficient (γ_{se}). As the change in the secondary electron coefficient (γ_{se}) as a function of the working pressure is not significant, the increase in voltage was consequently compensated by decreasing the ion current I_i, which is related to the discharge current I_d by [24]

$$I_d = (1+\gamma_{se})I_i. \quad (1)$$

For most metals, the value of secondary electron coefficient (γ_{se}) is ~0.05–0.2 for ion energies encountered in magnetron sputtering. Hence the dominating fraction of the discharge current at the target must be the ion current [25]. The observed values of the discharge current and the target voltage at a constant power of 300 W are given in table 1. Nitrogen added argon magnetron discharge contains Ar atoms (in ground state gs and excited metastable states Ar_m^+ at energy 11.2 eV), Ar^+ ions, several nitrogen species ($N^+, N_2{}^+, N_3^+, N_4^+$), the gs N atoms, as well as N2 molecules in gs and in various electronically excited levels [26, 27]. When hydrogen is added to nitrogen added argon plasma, the presence of the several hydrogen species including H^+, H_2^+, H_3^+ ions; ArH^+ ions, the gs H atom, gs H_2 molecule and various electronically excited states of H_2 molecules in the plasma is reported [28, 29]. Once

Table 2. Rate coefficients of different reactions in the plasma.

Equation no.	Reaction	Rate coefficient ($cm^3\ s^{-1}$)
2	$e^- + ArH^+ \rightarrow Ar + H$	1.0×10^{-7}
3	$e^- + H_3^+ \rightarrow H + H + H$	1.9×10^{-8}
4	$e^- + H_2^+ \rightarrow H + H$	1.0×10^{-7}
5	$Ar^+ + H_2 \rightarrow Ar(fast) + H_2^+$	8.0×10^{-11}
6	$ArH^+ + H_2 \rightarrow Ar(fast) + H_3^+$	1.5×10^{-9}
7	$e^- + H \rightarrow e^- + H^*$	4.3×10^{-8}
8	$e^- + H_2 \rightarrow e^- + 2H^*$	4.9×10^{-8}
9	$Ar^+ + H_2 \rightarrow ArH^+ + H$	6.0×10^{-10}

created, all the species of Ar/N2/H2 plasma mentioned above undergo different chemical reactions with different rate constants and relative cross sections. The important reactions with their respective rate coefficient that can influence the density variations in the plasma are given in table 2.

Electron impact ionization of Ar and H_2, and electron impact dissociative ionization of H_2 are the main production channels of Ar^+ and hydrogen related ions in the plasma. The loss of ions in the plasma occurs by ambipolar diffusion, but the removal by electron ion recombination (equations (2)–(4) in table 2) is also very important for molecular ions. For typical low pressure plasma with density $10^{15}\ m^{-3}$ and electron temperature greater than 2.5 eV, the recombination rate for molecular ions [30, 31] is indeed comparable with the diffusion loss rate [32, 33]. For the density values of ArH^+ and hydrogen ions, the values of recombination reaction rates turn out to be $7.6 \times 10^7\ s^{-1}$ and $1.19 \times 10^7\ s^{-1}$, respectively. But for atomic ions, the probability of electron ion recombination is very low. For example, the reaction rate coefficient of Ar^+ ion recombination is only $(1–0.01) \times 10^{-10}\ cm^3\ s^{-1}$. Smith and Cromey [32] have measured ambipolar diffusion coefficient of Ar^+ in the background of argon plasma and its value was $55\ cm^2\ s^{-1}$ Torr. Using this value of ambipolar diffusion coefficient the loss rate for Ar^+ ion in our case is found to be $1.834 \times 10^8\ s^{-1}$, which is much higher than the recombination rate for Ar^+ ion ($1.834 \times 10^4\ s^{-1}$). It is not always easy to find out the diffusion coefficient of ArH^+ ion in the background of such multi-component plasma. Therefore if we make quick order of magnitude estimate, the rate of recombination for ArH^+ ion ($\approx 10^7 s^{-1}$) is certainly comparable with its diffusion loss rate ($\approx 10^8 s^{-1}$). The recombination rate for H_3^+ ion ($1.19 \times 10^7\ s^{-1}$) is also comparable with its diffusion loss rate ($2.92 \times 10^7\ s^{-1}$) [32]. Additionally, the diffusion process for Ar^+ and ArH^+ in such plasmas gets slowed down in the presence of their parent gas because of the resonant charge transfer (Ar^+/Ar) or symmetrical proton transfer (ArH^+/Ar) (equations (5)–(6) in table 2) [28, 34]. Thus the loss of atomic ion due to diffusion is greater than the recombination loss rate but in case of molecular ions the diffusion loss is comparable with the recombination loss.

The reduction of density of Ar^+ ion due to addition of hydrogen has been observed by several authors [29, 35, 36]. Although the discharge conditions vary from one to another, the lost ionization was attributed to the inducement of fast recombination rates of molecular ions by one route or another. For example, Meulenbrecks *et al* [37] proposed that it occurs via the ion–molecule reaction to form ArH^+ (equation (9) in table 2). Since ArH^+ has a recombination coefficient many orders of magnitude larger than Ar^+, it is presumed to be rapidly removed from the plasma according to the equation (2). The densities of hydrogen related ions such as H^+, H_2^+, H_3^+ and ArH^+ are expected to increase with H_2 addition for obvious reasons. The effect is most pronounced for H^+, H_2^+, H_3^+ ions and is slightly less significant for ArH_+ ions.

In figure 2 intensity variation of the species of Ar I $[3s^23p^5(2p^0_{3/2})4s] \rightarrow [3s^23p^5(2p^0_{1/2})\ 4p]$ at 696.54 nm, 738.39 nm, 801.47 nm, 811.53 nm; Ar I $[3s^23p^5(2p^0_{1/2})4s] \rightarrow [3s^23p^5(2p^0_{1/2})\ 4p]$ at 751.5 nm, 763.51 nm, 772.37 nm, 794.81 nm, 826.45 nm, 840.82 nm, 852.14 nm; Ar II $[3s^23p^4(^3p)4s] \rightarrow [3s^23p^4(^3p)\ 4p]$ at 434.80 nm, 454.50 nm, 472.68 nm, 476.48 nm, 480.60 nm; H_α line (656.82 nm) and H_β line (487.54 nm); $N_2^+(B^2\Sigma_u^+ \rightarrow X^2\Sigma_g^+)$ at 391.58 nm and $N_2(C^3\Pi_u \rightarrow B^3\Pi_g)$ at 356.85 nm; Ti I line at 499.5 nm, and 510.53 nm are visible. Figure 2(b) shows zoom-in of the spectra from 340 nm to 500 nm. To a good approximation in low pressure discharge, the emission intensity of a particular line of an element can be considered to be proportional to the density of that particular species [38, 39]. Two neutral excited species of Ar at 751.5 nm and 811.53 nm respectively, Ar^+ excited ion at 476.4 nm as well as two neutral excited species of hydrogen at 656.82 (H_α) and 486.7 (H_β) nm have been selected for the qualitative analysis of density variation in hydrogen added N_2/Ar plasma. The impact of hydrogen partial pressure on the intensity (I) ratio of the 656.8 nm hydrogen atomic line to 751.5 nm argon line is shown in figure 3. The intensity ratio of the lines of excited species of Ar^+ to Ar (751.5 nm) is also given in the figure 3. The variation in the ratio of excited species of Ar^+ to Ar represents the trend of modulation of Ar^+ ion concentration in such plasma. It is clear that with increasing hydrogen partial pressure, the Ar^+ ion density decreases. Excited neutral hydrogen atoms (H∗) in such a plasma are produced by various recombination processes of hydrogen-related ions (equations (3) and (4) in table 2) and the electron impact excitation of hydrogen or dissociative excitation of H_2 (equations (7) and (8) in table 2) [28, 40]. But for such low pressure plasma the degree of dissociation of hydrogen for DC discharges is less than 0.01 percent and therefore, its dissociative excitation rate is much slower compared to recombination excitation [41, 42]. Thus, H_α characteristic emission line at 658.6 nm could be used as a representative of relative density of hydrogen related ions in such plasma. With addition of hydrogen, the intensity ratio of the lines of excited species of H_α (658.6 nm) to Ar (751.5 nm) increases gradually. This clearly indicates an increase of hydrogen-related ions when the hydrogen partial pressure is increased.

It is worthwhile to mention that hydrogen addition in N_2 + Ar plasma leads to changes in the I–V plot obtained from Langmuir probe measurements, and thus the plasma parameters obtained from the I–V characteristics begin to change. The electron density and electron temperature are plotted as a function of hydrogen partial pressure. Addition of hydrogen to

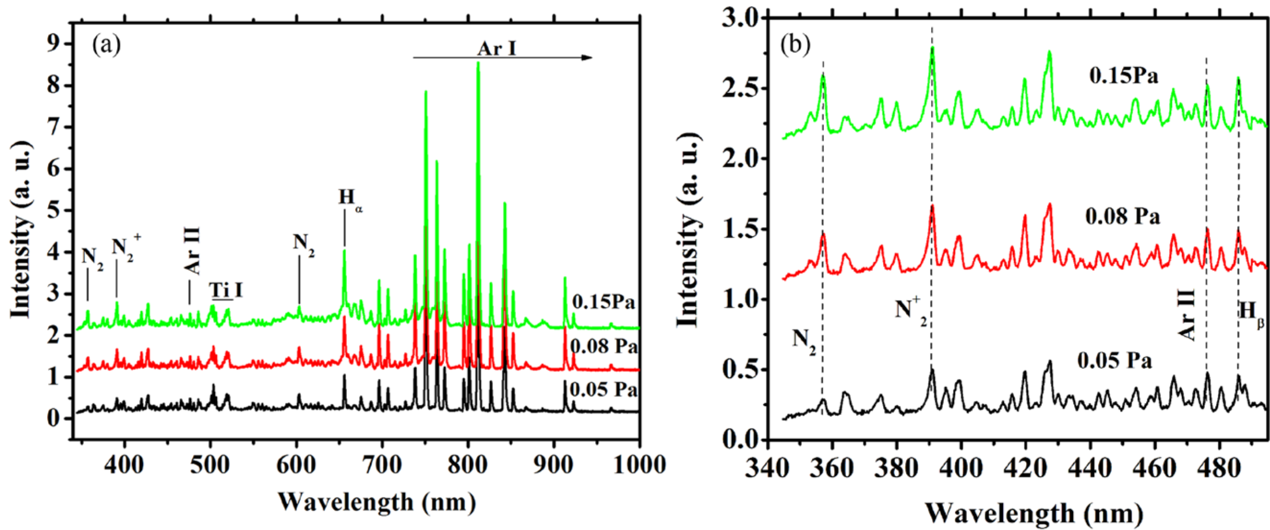

Figure 2. (a) Spectral emission lines collected for the hydrogen added nitrogen containing argon plasma at three different working pressures; (b) zoom of the spectra from 340 nm to 500 nm.

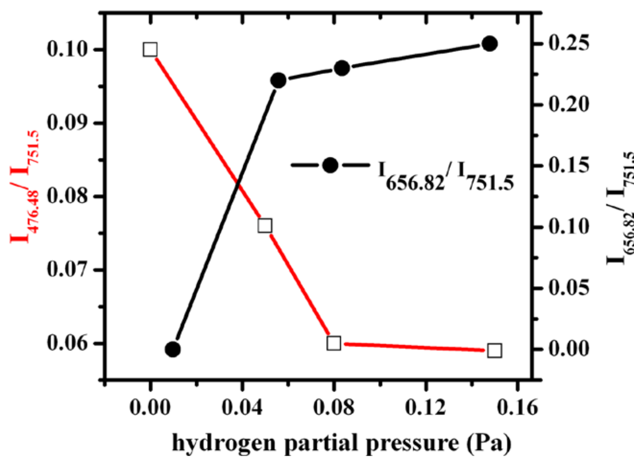

Figure 3. Influence of hydrogen partial pressure on the intensity (I) ratio of the 656.8 nm hydrogen atomic line to the 751.5 nm argon line and the 476.48 nm argon ion line to the 751.5 nm argon line.

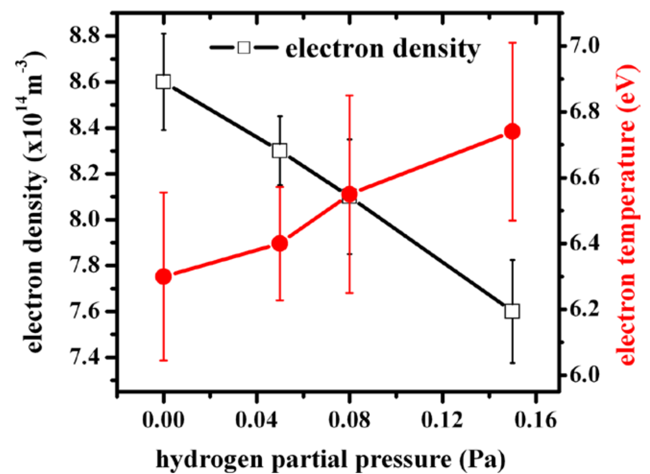

Figure 4. Influence of hydrogen partial pressure on electron density and temperature.

nitrogen containing argon plasma leads to a decrease of electron density from 8.6 to 6.2 ($\times 10^{14}$ m^{-3}) and a corresponding increase of electron temperature from 6.30 to 6.74 eV (see figure 4). It is interesting to mention that increase in electron temperature can be accounted for the reduction of the electron density in this regime. As the Ar/H_2 plasma contains various ion species (Ar^+, ArH^+, N^+, N_2^+, N_3^+, N_4^+, H^+, H_2^+, H_3^+ etc), it is not possible to determine the density of each ion individually using the Langmuir probe. Moreover, due to the presence of these ionic species, the use of argon ion mass in the ion density calculation is not valid. As the partial pressure of N_2 is lower than argon partial pressure, we have not included the contribution of nitrogen containing ions (N^+, N_2^+, N_3^+, N_4^+) in the ion density calculation. Then, we can classify the remaining ions into two groups. A heavy group of mass 40 amu that consists of Ar^+ and ArH^+ ions, and a light group of mass 2 amu which consists of hydrogen related ions (H^+, H_2^+, and H_3^+ ions). Following the mean ion mass procedure as developed by Laidani *et al* [43], we have calculated the density of each group of ions and are shown in the figure 5. It is interesting to note that while the heavy ion density in the discharge is inversely proportional to the hydrogen enrichment in the feeding gas, the hydrogen related ion density scales linearly with it.

3.2. Thin film analysis

Figure 6 shows XPS spectrum of broad energy scan obtained from a TiN coated substrate with hydrogen partial pressure of 0.05 Pa. It is to be mentioned here that no major differences are detected in the spectra obtained from the coated substrates with and without the presence of H_2 (not shown in the figure). All the spectra show photoelectron and auger signals from Ti (Ti 2s, Ti 3s, Ti 3p, Ti LMM), Nitrogen (N 1s, N KLL), oxygen (O 1s, O KLL) and spurious carbon (C 1s). The presence of oxide on the deposited TiN film is most likely due to the presence of oxygen in the deposition chamber. Also when the coated substrates were taken out from the deposition chamber and exposed to air, passivating layers of native oxide may grow on the thin film.

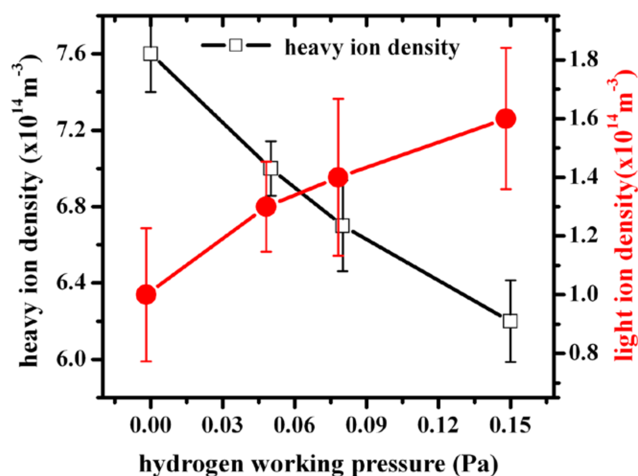

Figure 5. Effect of hydrogen partial pressure on the density of heavy and light ions in the discharge

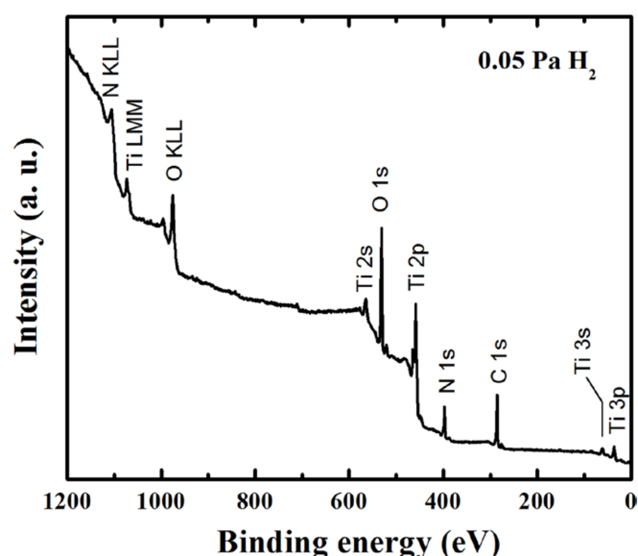

Figure 6. XPS spectrum of broad energy scans from a coated substrate under a hydrogen partial pressure of 0.05 Pa.

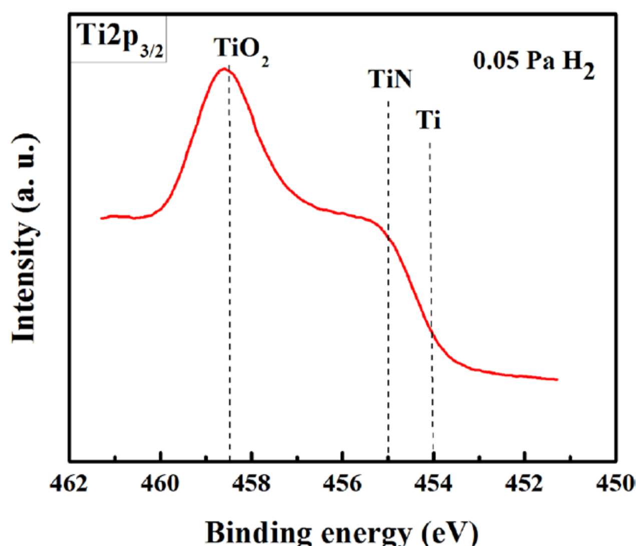

Figure 7. High resolution XPS spectrum of the Ti $2p_{3/2}$ signal from a coated substrate under a hydrogen partial pressure of 0.05 Pa.

Figure 7 shows high resolution XPS spectrum of the Ti $2p_{3/2}$ signal acquired from coated substrates at a hydrogen partial pressure of 0.05 Pa. Similar spectra were observed without and with H_2 (not shown in the figure). All Ti $2p_{3/2}$ spectra reveal a shoulder with a binding energy (BE) around 455.0 eV attributed to the formation of TiN and a well-defined peak with a BE around 458.4 eV attributed to the presence of a oxide layer of type TiO_2 (Ti(IV)–O bond). These binding energy values are close to the reported ones in the literature for TiN_xO_y and TiN [29, 34]. The dotted line in figure 7 around 454.0 eV reveals the BE value of metallic Ti as a reference. Therefore, the shift to higher energies indicates the formation of the TiN coating on the substrates. However, no significant changes of binding energy are detected in the Ti $2p_{3/2}$ spectra of the samples deposited at different hydrogen partial pressures.

Figure 8 shows the intensity ratios between the main photoelectron signal of N (N 1*s*) or Ti (Ti $2p_{3/2}$) to O (O 1*s*) as well as the intensity ratios between the signals of Ti to N. In general, figure 8 shows similar intensity ratios among the samples revealing that no significant changes of surface chemical composition are obtained between the samples grown without hydrogen, (1) and (2), and the ones grown with hydrogen addition in the N_2/Ar plasma. Only sample (3), grown under a H_2 partial pressure of 0.05 Pa, showed a chemical change slightly more evident. The value of the intensity ratio of Ti to N (framed with a circle in figure 8) for this sample is slightly more significant compared to the values obtained from the other samples. The values of the N/O ratios (between 0.3 and 0.5) are less than the values of Ti/O ratios (between 0.9 and 1.1) corroborating the presence of a titanium oxide layer on the TiN coating, as revealed in figure 7. For the same reason, the Ti/N ratios of all the samples have values higher than 1. The presence of oxide on the TiN coating was also corroborated by the curve fitting results obtained from the high resolution XPS spectra of O 1*s* signal.

Figure 9 shows the comparison of the x-ray diffraction patterns of the coated substrates without and with hydrogen partial pressure of 0.15 Pa for two different deposition times i.e. 30 min and 60 min. All the diffraction patterns show peaks with 2θ at 33°, 36.6°, 42.7° and 61.4°. The diffraction peak at around $2\theta = 33°$ belongs to the silicon substrate and the peaks at $2\theta = 36.6°$, 42.7° and 61.4° correspond, respectively, to the (1 1 1), (2 0 0) and (2 2 0) planes of TiN thin film. At 61.4° the TiN (2 2 0) is overlapping with the Cu K_β radiation scattered at the Si (4 0 0) substrate reflections. Additionally, Ti_2N and rutile TiO_2 are present for some samples while no anatase or metallic Ti has been observed. It is observed that the diffraction peaks of (2 2 0) is shifted slightly toward the higher angle for the substrates deposited with the addition of hydrogen as shown in the insert of the figure 9. It indicates a decrease of compressive stress as compared to the reference sample (deposited without hydrogen). This is probably due to lowering of ion bombardment on the growing thin film [44]. In order to establish this result, the total ion current to the substrate was measured at various deposition conditions.

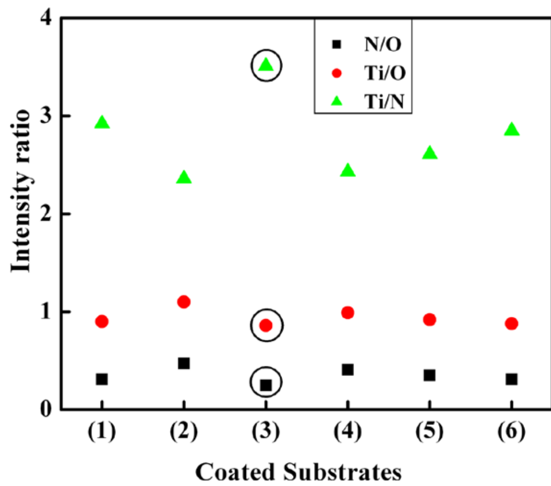

Figure 8. The intensities ratio between the main photoelectron signals of N (N 1*s*) or Ti (Ti $2p_{3/2}$) and O (O 1*s*) as well as the intensities ratio between the signal of Ti and N from each sample. (1) Ar/N_2, 30 min (2) Ar/N_2, 1 h (3) 0.05 Pa H_2 (4) 0.08 Pa H_2 (5) 0.1 Pa H_2 (6) 0.15 Pa H_2.

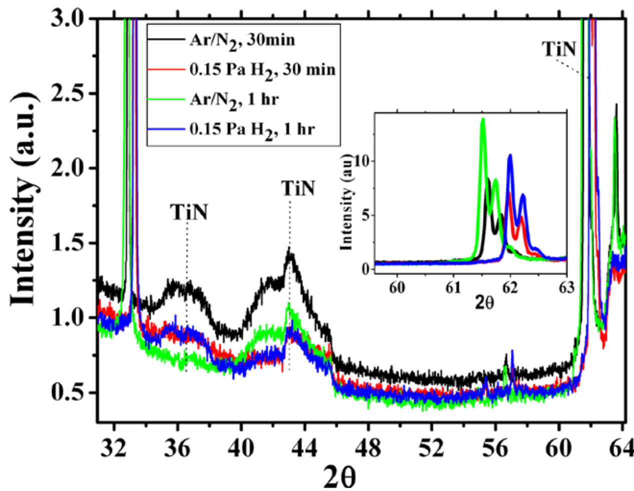

Figure 9. XRD patterns of the coated substrates without and with hydrogen partial pressure of 0.15 Pa for two different deposition times.

For this, the substrate holder was used as a planar Langmuir probe and biased at −30 V to obtain the ion saturation current. The measured value of ion current density to the substrate decreases from 1.27–1.12 Am^{-2} as the hydrogen partial pressure increases from 0–0.15 Pa. The measured value of ion current density is typical of DC planar magnetron discharge (<1 mA cm^{-2}) [23]. It is also interesting to note that, the intensity of TiN (1 1 1) and TiN (2 0 0) peaks in the presence of hydrogen is less than that of the reference sample. This change is expected as the deposition rate decreases with the addition of hydrogen in nitrogen added argon discharge, resulting thinner TiN films.

Figure 10 shows Raman spectra of the coated substrates in different gas mixture for different deposition times. It is believed that the deposited films contain microscopic defects i.e. vacancies in sub-lattices (metal ions) including vacancies due to deficiency of nitrogen ions. This defect induces first order Raman scattering indicating that the perturbed

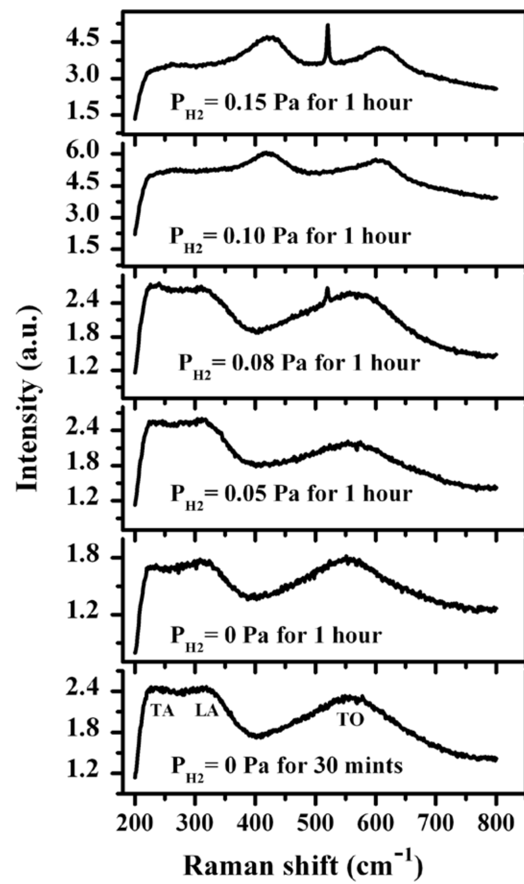

Figure 10. Raman spectra of the TiN coated substrates deposited without and with different hydrogen partial pressures (P_{H_2}).

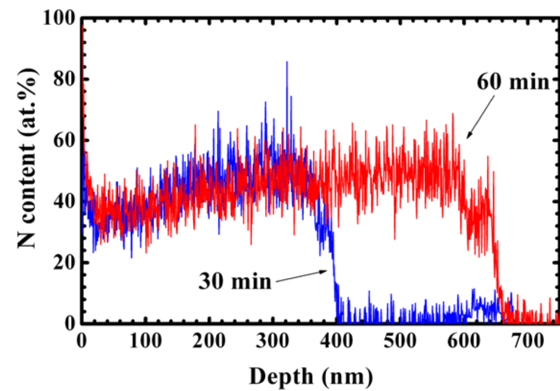

Figure 11. Depth profiles of nitrogen content in the coated substrates under a hydrogen partial pressure of 0.05 Pa for two different deposition time: 30 min (blue curve) and 60 min (red curve).

projected phonon density of states can be obtained from the three Raman-active modes [45, 46]. The Raman spectrum of TiN films can be fitted to four Gaussian–Lorentzian peaks at about 235, 320, 420 and 560 cm^{-1}. It was reported that the dispersion curves lead to a group of bands due to the acoustic transition in the 150–300 cm^{-1} region and another set of lines due to optical modes in the 400–650 cm^{-1} region [46]. In our case the peaks at 235, 320 and 560 cm^{-1} arise from first-order transverse acoustic (TA), longitudinal acoustic (LA), and transverse optical (TO) modes of TiN films, respectively.

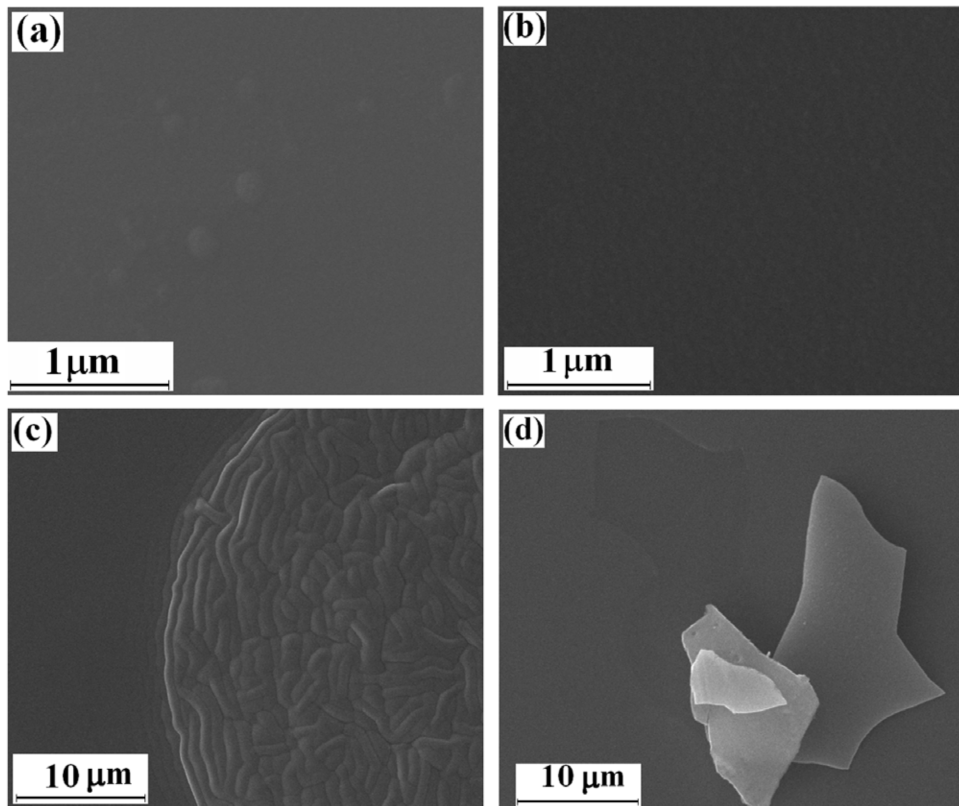

Figure 12. SEM micrographs of the coated substrates deposited using (a) admixture of N_2 and Ar for 30 min, (b) admixture of N_2 and Ar for 1 h, (c) with hydrogen partial pressure of 0.05 Pa for 1 h, and (d) with hydrogen partial pressure of 0.08 Pa for 1 h duration.

The peak at around 420 cm^{-1} arises from the second-order acoustic (2A) mode. This second order peak was observed on the coated substrates with H_2 partial pressure higher than 0.1 Pa.

It is proven that the scattering in the ion acoustic region is primarily determined by the vibration of the heavy titanium (Ti) ions and in the optic range by the vibration of the lighter nitrogen (N) ion [46]. However, the influence of the H_2 addition on the intensity variation pattern of the acoustic and the optical modes is not found to be significant. The intensity variation of the Raman peaks for TiN films is mainly attributed due to the variation of Ti/N ratio, as shown in figure 8. According to Spengler *et al* [46], decreases in deviation from the stoichiometry (N/Ti) ratio leads to the increase in the intensity of the Raman peaks. With the introduction of hydrogen in the nitrogen containing argon discharge, we observed a gradual decrease of the electron density as well as the degree of ionization which in turn reduces the sputtering rate. As such, a gradual decrease of both the Ti^+ and N^+ ion density are expected with increasing hydrogen content in the discharge. Therefore, it is reasonable to expect that the N/Ti ratio will not vary significantly due to hydrogen addition.

Rutile (TiO_2) has very prominent Raman modes including E_g and A_{1g} at 447 and 612 cm^{-1}, respectively [47]. Additionally, a broad, disorder induced mode around 250 cm^{-1} is often observed for nanocrystalline materials [48]. Using this interpretation, a transition towards TiO_2 containing films at high hydrogen partial pressures could be explained. Additional investigations using time-of-flight secondary ion mass spectrometry (ToF-SIMS) have been performed to clarify this situation. While the existence of a TiO_2 could be proven in this way, no information about the existence or absence of TiN within this film can be provided as the mode intensity is highly non-linear for the second order Raman process. However, the TiO_2 should be at least some kind of microcrystalline structure (to be differentiated from nanocrystallites which yield a different Raman signal) and it may not be buried below a non-transparent surface layer as both the exciting and scattered radiations would be absorbed within such a layer.

Hence, additional investigations by ToF-SIMS were carried out using reference TiN and TiO_2 samples produced by vacuum arc deposition [49] with typical nitrogen depth profiles and are shown in figure 11. However, the existence of very strong matrix effects deriving from the varying hydrogen addition (which was not present for the reference samples) may falsify these results. Thus, any absolute quantification of the results has to be regarded cautiously. Nevertheless, a relative comparison of the TiN layer thickness at two different deposition times is possible. It was observed that for 30 min deposition substrate the TiN layer thickness is around 400 nm while a layer thickness of 700 nm was observed for one hour deposited substrate as shown in figure 11. The thickness observed by SIMS measurements is well agreed with the results obtained from the Crystal Thickness Monitor mentioned in the experimental set-up. This slight implied time dependence of the deposition rate may actually point towards time dependent plasma effects, e.g. from a partial etching of the chamber walls after the transient addition of hydrogen.

SEM micrographs of the coated substrates using only an admixture of N_2 and Ar for different deposition time are shown in figures 12(a) and (b). The substrate coated for 1 h (figure 12(b)) shows a smooth surface compared to that with 30 min (figure 12(a)). A close view on the substrate surface, coated for 1 h reveals formation of nanostructures with uniform distributions. While comparing the EDS results, it is observed that the atomic percentage of titanium on the substrate coated for 1 h is much higher than for 30 min, the difference is 24.2%, whereas the difference in nitrogen content is only 9.3%. However, there is a strong peak overlap of nitrogen-*K* (392 eV) and titanium-Ll (395 eV) which cannot be separated using standard detectors with an energy resolution between 50 and 100 eV. Thus, the partitioning of the 'Ti + N' signal into Ti and N component is incurring a large error. On the other hand the silicon percentage is almost half in the case of the substrate coated for 1 h. This observation indicates that the substrate coated for 1 h is covered by a thick TiN layer compared to that of the 30 min, which is expected and correlates well with the SIMS results.

SEM micrographs of the plasma coated substrates for one hour in two different partial pressure of H_2 are shown in figures 12(c) and (d). While adding H_2 (at a partial pressure of 0.05 Pa and above) worm like structures are appeared in some zones (shown in figure 12(c)) on the surface. The atomic percentage of nitrogen decreases from 35.4% to 27.16%, whereas silicon percentage increases as a function of hydrogen addition. This probably indicates that the coated TiN film is thinner compared to the one without addition of H_2. Further increase in H_2 flow rate shows poor adhesion of the coatings to the substrate. In this case, we observed that in some zones the TiN layer is peeled off (at a partial pressure of 0.08 Pa) which can be seen in the SEM micrograph presented in the figure 12(d). Thus we observed that the H_2 addition in the N_2 + Ar magnetron plasma at the higher working partial pressures used in this research did not contribute to grow a higher quality TiN film.

As revealed by XPS results (figure 8), the H_2 addition did not reduce significantly the oxygen amount of the oxide layer formed on the TiN film and only led to deteriorate the film, as shown by aforementioned SEM images. It is known that in metals the hydrogen diffuses mainly into grain boundaries. At higher flow rates, the plasma density decreases and thus the ion bombardment for ion mixing during the initial deposition phase and the stress relaxation during the film growth is reduced [50]. The high H_2 presence in grain boundaries generates local stresses reducing the ductility of the material. It is speculated that in our case we have a similar effect. The H_2 diffuses mainly into grain boundaries of TiN generating stresses not only inside the thin film but also with the Si substrate. These stresses increase the lattice mismatch between the grains of TiN and the substrate in the interphase zone, reducing the adhesion and/or generating delamination of the film. In summary, probably for a better quality and non-delamination of the coating to the substrate a smaller but finite percentage of hydrogen is required. More investigation needs to be carried out even with lower hydrogen partial pressure (less than 0.05 Pa) to clarify the effect.

4. Conclusions

The effect of hydrogen addition to the nitrogen containing argon plasma on the bulk plasma properties and structural properties of the deposited TiN thin film is discussed. The Langmuir probe and the OES study reveal a gradual decrease of electron density (8.6×10^{14}–7.5×10^{14} m^{-3}) and heavy ion density (7.6×10^{14}–6.2×10^{14} m^{-3}) which in turn decreases the deposition rate (2.6 Å s^{-1} to 2.1 Å s^{-1}) as a function of hydrogen addition. XPS, XRD and RS confirm the formation of TiN films on silicon substrates while other phases may be present at certain deposition conditions. Shifting of TiN (2 2 0) peaks towards higher diffraction angle indicates the decrease of compressive stress upon hydrogen addition to the nitrogen added argon magnetron discharge. The spectral intensity of the Raman peaks is not found to be varying significantly with hydrogen addition. SEM and EDS results shows that the thickness of the TiN films decreases and also the films quality deteriorates (poor adhesion) while increasing hydrogen partial pressure from 0 to 0.15 Pa.

Acknowledgments

Authors acknowledge FONDECYT grant 1130228 and FONDECYT grant 3160179. Additional funding from Conicyt PIA program ACT1108 is also acknowledged.

References

[1] Ehiasarian A P, Vetushka A, Aranda Gonzalvo Y, Sáfrán G, Székely L and Barna P B 2011 *J. Appl. Phys.* **109** 104314
[2] Martínez-Martínez D, López-Cartes C, Fernández A and Sánchez-López J C 2013 *Appl. Surf. Sci.* **275** 121
[3] Patsalas P, Charitidis C and Logothetidis S 2000 *Surf. Coat. Technol.* **125** 335
[4] Solovana M N, Brusa V V, Maistruka E V and Maryanchuk P D 2014 *Inorg. Mater.* **50** 40
[5] Fu Y, Du H and Zhang S 2003 *Surf. Coat. Technol.* **167** 129
[6] Liu X, Chu P K and Ding C 2004 *Mater. Sci. Eng.* R **47** 49
[7] Mishnaevsky L Jr *et al* 2014 *Mater. Sci. Eng.* R **81** 1
[8] van Hove R P, Sierevelt I N, van Royen B J and Nolte P A 2015 *Biomed. Res. Int.* **2015** 485975
[9] Dienelt J, Zimmer K and Neumann H 2003 *Surf. Coat. Technol.* **174–5** 157
[10] Budtz-Jorgensen C V, Kringhoi P, Nelson J F and Bottinger J 2002 *Surf. Coat. Technol.* **135** 299
[11] Budtz-Jorgensen C V, Kringhoi P and Bottinger J 1999 *Surf. Coat. Technol.* **116** 938
[12] Tsuij K and Hirokawa K 1991 *Thin Solid Film* **205** 6
[13] Popescu B, Verney C, Davis E A, Paret V and Brunet-Bruneau A 2000 *J. Non-Cryst. Solids* **266** 778
[14] Popescu B, Trgliaferro A, De Zan F and Davis E A 2000 *J. Non-Cryst. Solids* **266** 803
[15] Park J S, Lee M J, Lee C S and Kang S W 2001 *Electrochem. Solid-State Lett.* **4** C17
[16] Buha J 2013 *Thin Solid Films* **545** 234
[17] Wang F H, Yang C F, Liou J C and Chen I C 2014 *J. Nanomater.* **2014** 857614
[18] Jang C, Ye Z and Jiang Q 2015 *Mater. Sci. Semicond. Process.* **30** 152
[19] Saikia P, Kakati B and Saikia B K 2013 *J. Vac. Sci. Technol.* **31** 0613071

[20] Saikia P, Saikia B K, Goswami K S and Phukan A 2014 *J. Vac. Sci. Technol.* **32** 031303
[21] Sahu B B, Han J G, Hori M and Takeda K 2015 *J. Appl. Phys.* **117** 023301
[22] Bundesmann C, Feder R, Wunderlich R, Teschner U, Grundmann M and Neumann H 2015 *Thin Solid Films* **589** 487
[23] Kelly P J and Arnell R D 2000 *Vacuum* **56** 159
[24] Depla D, Buyle G, Haemers J and De Gryse R 2006 *Surf. Coat. Technol.* **200** 4329
[25] Maniv S and Westwood W B 1980 *J. Vac. Sci. Technol.* **17** 743
[26] Bogaerts A 2009 *Spectrochim. Acta* B **64** 126
[27] Rejoub R, Lindsay B G and Stebbings R F 2002 *Phys. Rev.* A **65** 042713
[28] Bogaerts A and Gijbels R 2002 *Phys. Rev.* E **65** 056402-1
[29] Knewstubb P F and Tickner A W 1962 *J. Chem. Phys.* **36** 674
[30] Dexter A C, Farrell T and Lees M I 1983 *J. Phys. D: Appl. Phys.* **22** 413
[31] Kawara H, Itikara Y, Nishimura H and Yoshino M 1990 *J. Phys. Chem. Ref. Data* **19** 617
[32] Smith D and Cromey P R 1968 *J. Phys. B: At. Mol. Phys.* **1** 650
[33] Ellis H W, Pai R Y and Mcdaniel E W 1976 *At. Data. Nucl. Data Tables* **17** 177–210
[34] McDaniel E W 1973 *Mobility and Diffusion of Ions* (New York: Wiley)
[35] Gordon M H and Kruger C H 1993 *Phys. Fluids* B **5** 1014
[36] DeGraaf M J, Severens R J, Dahiya R P, Van deSanden M C M and Schram D C 1992 *Phys. Rev.* E **48** 2098
[37] Meulenbroeks R F G, Van Beek A J, Helvoort A J G, Van de Sanden M G M and Schram D C 1994 *Phys. Rev.* E **49** 4397
[38] Coburn J W and Chen M 1980 *J. Appl. Phys.* **51** 3134
[39] Zambrano G, Riascos H, Prieto P, Restrepo E, Devia A and Rincon C 2003 *Surf. Coat. Technol.* **172** 144
[40] Otorbaev D K, Buuron A J M, Guerassimov N T, van de Saden M C M and Schram D C 1994 *J. Appl. Phys.* **76** 4499
[41] Lavrov B P, Lang L, Pipa A V and Roopke J 2006 *Plasma Sources Sci. Technol.* **15,** 147
[42] Rahman M A, Gathen V, Gans T, Niemi K and Dobele H F 2006 *Plasma Sources Sci. Technol.* **15** 620
[43] Laidani N, Bartali R, Tosi P and Anderle M 2004 *J. Phys. D: Appl. Phys.* **37** 2593
[44] Akamaru S, Honda Y, Taguchi A and Abe T 2008 *Mater. Trans.* **49** 1638
[45] Montgomery G P, Klein M V, Ganguly B N and Wood R F 1972 *Phys. Rev.* B **6** 4047
[46] Spengler W, Kaiser R, Christensen A N and Muller-Vogt G 1978 *Phys. Rev.* B **17** 1095
[47] Mändl S, Thorwarth G, Schreck M, Stritzker B and Rauschenbach B 2000 *Surf. Coat. Technol.* **125** 84
[48] Balachandran U and Eror N G 1982 *J. Solid State Chem.* **42** 276
[49] Asenova I, Manova D and Mändl S 2014 *J. Phys.: Conf. Series* **559** 012008
[50] Manova D, Attenberger W, Mändl S, Stritzker B and Rauschenbach B 2004 *J. Vac. Sci. Technol.* A **22** 2299